LAWRENCE
LIVERMORE
NATIONAL
LABORATORY

UCRL-TR-226999

Simulation and Comparison of Various Gamma-Ray Imaging Detector Configurations for IPRL Devices

H. A. Manini

December 27, 2006

This work was performed under the auspices of the U.S. Department of Energy by University of California, Lawrence Livermore National Laboratory under Contract W-7405-Eng-48.

h4doc IPRLv1
UCRL-TR-226999

Simulation and Comparison of Various Gamma-Ray Imaging Detector Configurations for IPRL Devices

Hugh Manini

N Division
Lawrence Livermore National Laboratory

May 24, 2006

Abstract

Simulations are performed for seven different geometrical configurations of CdZnTe (CZT) detector arrays for Intelligent Personal Radiation Locator (IPRL) devices. IPRL devices are portable radiation detectors that have gamma-ray imaging capability. The detector performance is analyzed for each type of IPRL configuration, and the intrinsic photopeak efficiency, intrinsic photopeak count rate, detector image resolution, imaging efficiency, and imaging count rate are determined.

1 Detector simulations

I perform full physics simulations using GEANT4 of each type of IPRL detector configuration. Seven different types of IPRL detector configurations are simulated. Each configuration is an array of CZT detectors.

Each GEANT4 simulation is run once for each specific detector geometry. Source photons from a point source are generated at a specific energy and tracked through the detector volumes. The positions and energies for each interaction are stored for further analysis. The exact information is then "digitized", and detector resolution effects are introduced, so that the resulting simulated output mimics the realistic detector response. The exact x and y coordinates of the interactions within the active detector crystals are pixelized. Each detector array has pixels in the xy-plane that are each 2.5 mm$\times$2.5 mm in size (the xy-plane is parallel to the front surface of each detector crystal), except for the $2\times2\times2$ array of 25 mm$\times$25 mm$\times$5 mm CZT detectors, which has pixels that are each 1.56 mm$\times$1.56 mm in size. When more than one interaction occurs within a pixel, the interactions and deposited energies are combined. The detected energy distribution is determined by smearing individual energy deposits using a Gaussian probability distribution with a specified FWHM at each energy, to model the energy resolution. The interaction depth within the detector is represented by the z coordinate, and two different types of z resolution are considered. The first type of z resolution is modeled by smearing the exact z coordinate of each interaction using a Gaussian probability distribution with a FWHM of 1 mm. The second type of z resolution model replaces the exact z coordinate of each interaction with the z coordinate of the center of the CZT detector which contains the interaction.

1.1 Simulated detector geometry for 1×2×2 array of CZT detectors

The simulated detector geometry for each 1×2×2 array of CZT detectors includes one row of CZT detectors in the *x* direction, two rows in the *y* direction, and two rows in the *z* direction. Two different types of 1×2×2 arrays are simulated. One type uses CZT detectors which are 20 mm×20 mm×5 mm in size. The other type uses CZT detectors which are 20 mm×20 mm×7.5 mm in size. For each type of array, each CZT detector has a thin layer of inactive CZT around the side edges which is 0.1 mm wide. The simulated detector geometry for a 1×2×2 array is shown in Figure 1.

1.2 Simulated detector geometry for 2×2×1 array of CZT detectors

The simulated detector geometry for each 2×2×1 array of CZT detectors includes two rows of CZT detectors in the *x* direction, two rows in the *y* direction, and one row in the *z* direction. Two different types of 2×2×1 arrays are simulated. One type uses CZT detectors which are 20 mm×20 mm×5 mm in size. The other type uses CZT detectors which are 20 mm×20 mm×7.5 mm in size. For each type of array, each CZT detector has a thin layer of inactive CZT around the side edges which is 0.1 mm wide. The simulated detector geometry for a 2×2×1 array is shown in Figure 2.

1.3 Simulated detector geometry for 2×2×2 array of CZT detectors

The simulated detector geometry for each 2×2×2 array of CZT detectors includes two rows of CZT detectors in the *x* direction, two rows in the *y* direction, and two rows in the *z* direction. Three different types of 2×2×2 arrays are simulated. One type uses CZT detectors which are 20 mm×20 mm×5 mm in size. The second type uses CZT detectors which are 20 mm×20 mm×7.5 mm in size. The third type uses CZT detectors which are 25 mm×25 mm×5 mm in size. For each type of array, each CZT detector has a thin layer of inactive CZT around the side edges which is 0.1 mm wide. The simulated detector geometry for a 2×2×2 array is shown in Figure 3.

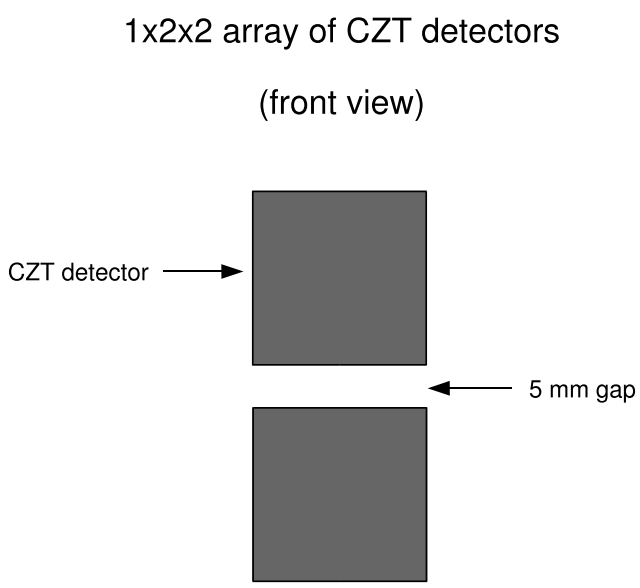

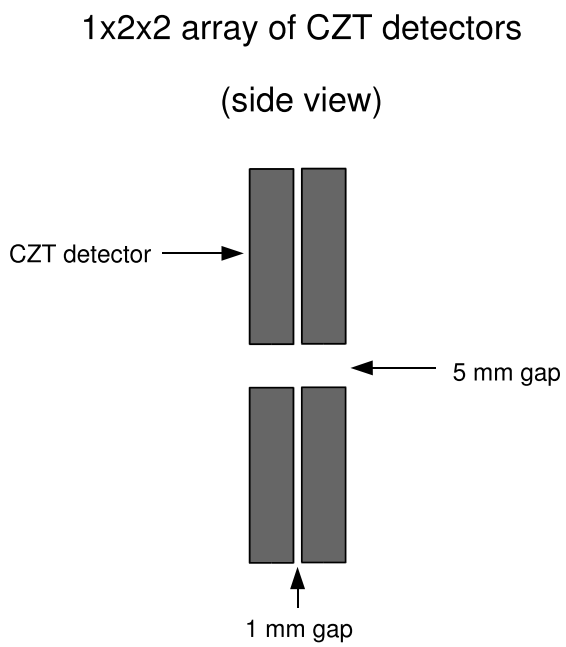

Figure 1: Simulated detector geometry for the $1\times2\times2$ array of CZT detectors.

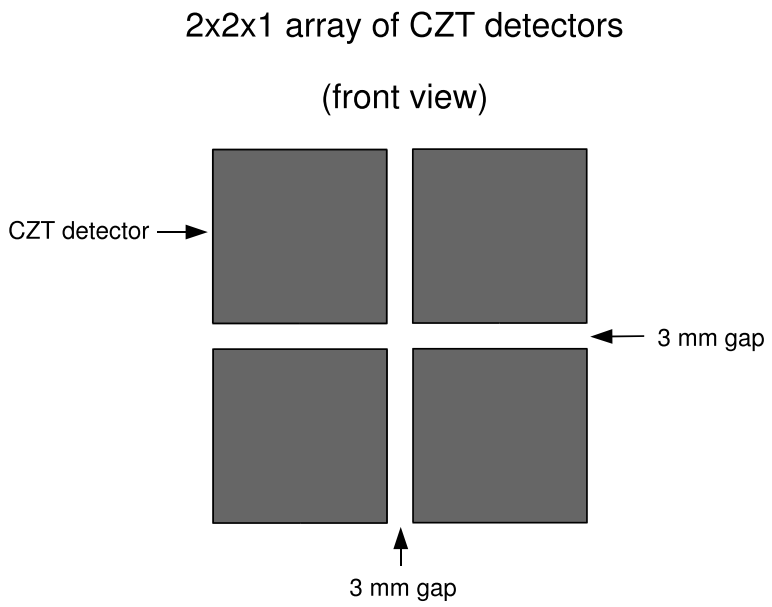

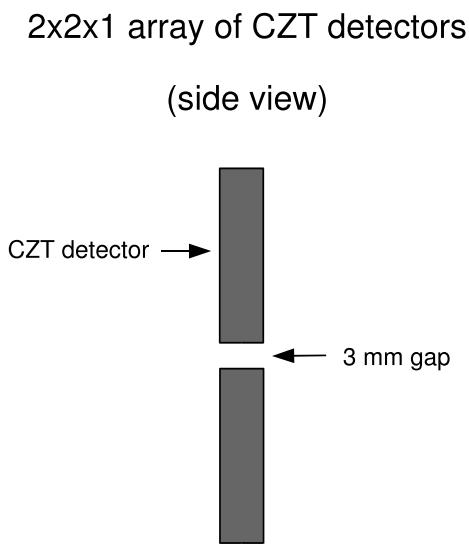

Figure 2: Simulated detector geometry for the $2\times2\times1$ array of CZT detectors.

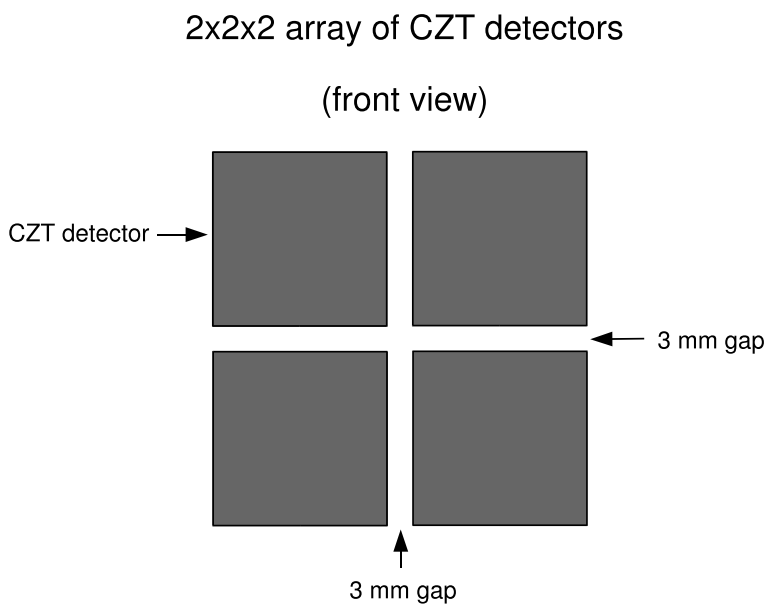

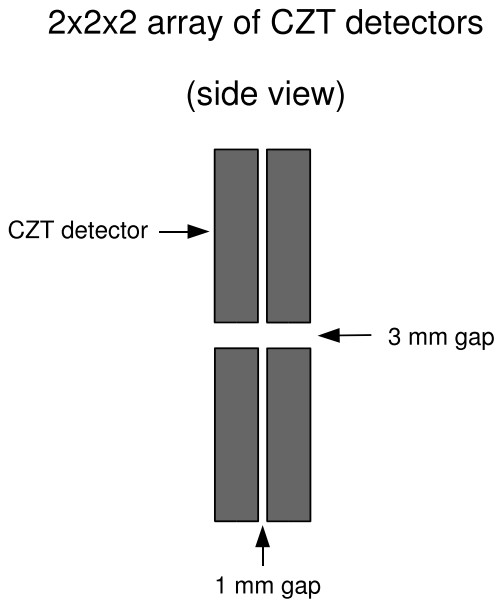

Figure 3: Simulated detector geometry for the $2\times2\times2$ array of CZT detectors.

2 Energy resolution model

The energy resolution model used for the CZT detectors is based on measured CZT data. To model the energy resolution, individual energy deposits are smeared using a Gaussian probability distribution with a specified FWHM at each energy. The energy resolution model for the CZT detectors is shown in Figure 4.

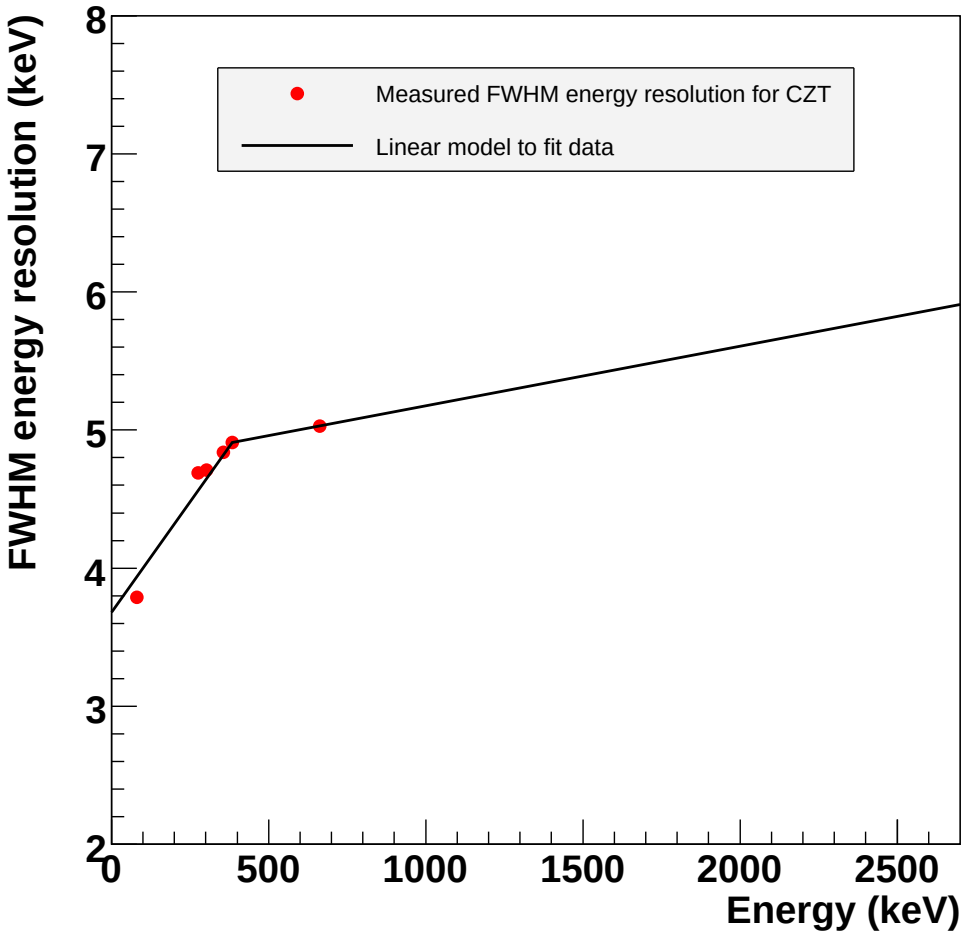

Figure 4: Energy resolution for CZT detectors.

3 Intrinsic photopeak efficiency

The intrinsic photopeak efficiency at a particular energy is the number of detected events within a ± 13 keV energy window, divided by the total number of events incident upon the detector array at the particular energy. Table 1 shows the results for the intrinsic photopeak efficiency at 662 keV for each type of detector array. These results show that the CZT detectors which are 7.5 mm thick produce significantly better intrinsic photopeak efficiency than the CZT detectors which are 5 mm thick. Figure 5 shows the intrinsic photopeak efficiency versus energy for the $2\times2\times2$ array of 20 mm$\times$20 mm$\times$5 mm CZT detectors.

Detector array type	Intrinsic photopeak efficiency at 662 keV
$1\times2\times2$ array with 20mm$\times$20mm$\times$5mm CZT detectors	10.3 %
$1\times2\times2$ array with 20mm$\times$20mm$\times$7.5mm CZT detectors	15.8 %
$2\times2\times1$ array with 20mm$\times$20mm$\times$5mm CZT detectors	4.8 %
$2\times2\times1$ array with 20mm$\times$20mm$\times$7.5mm CZT detectors	7.9 %
$2\times2\times2$ array with 20mm$\times$20mm$\times$5mm CZT detectors	10.9 %
$2\times2\times2$ array with 20mm$\times$20mm$\times$7.5mm CZT detectors	17.2 %
$2\times2\times2$ array with 25mm$\times$25mm$\times$5mm CZT detectors	11.5 %

Table 1: Intrinsic photopeak efficiency at 662 keV, for each type of detector array.

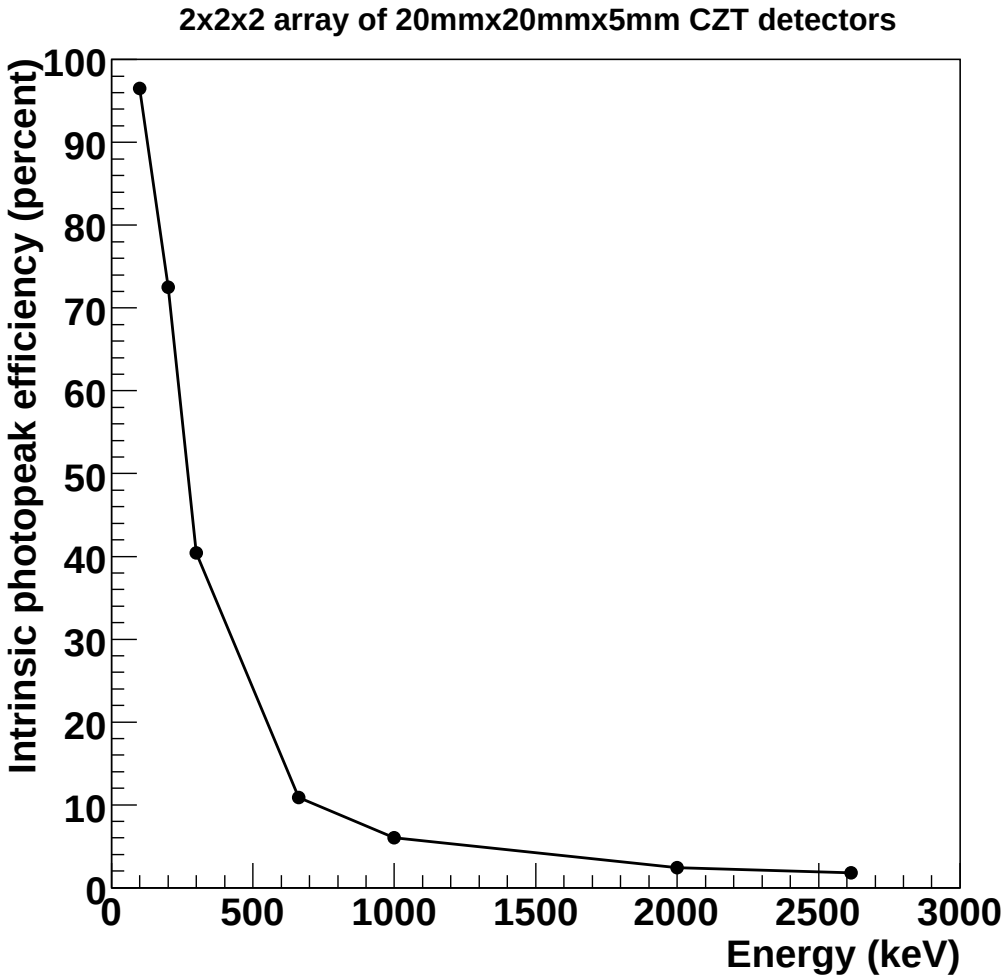

Figure 5: Intrinsic photopeak efficiency versus energy for the $2\times2\times2$ array of 20 mm$\times$20 mm$\times$5 mm CZT detectors.

4 Intrinsic photopeak count rate

Table 2 shows the results for the intrinsic photopeak count rates at 662 keV for each type of detector array, for a 1 mCi ^{137}Cs source located 10 meters away from the detector array, on the center axis of the detector array. These results include the fact that the branching ratio is 85% for a ^{137}Cs decay to emit a 662 keV photon. Note that at a distance of 10 meters, a 1 mCi ^{137}Cs source generates 662 keV photons at a rate of 2.50 photons/second/cm^2. These results show that the CZT detectors which are 7.5 mm thick produce significantly better intrinsic photopeak count rates than CZT detectors which are 5 mm thick.

Detector array type	Intrinsic photopeak count rate at 662 keV (counts/second)
1×2×2 array with 20mm×20mm×5mm CZT detectors	2.06
1×2×2 array with 20mm×20mm×7.5mm CZT detectors	3.16
2×2×1 array with 20mm×20mm×5mm CZT detectors	1.92
2×2×1 array with 20mm×20mm×7.5mm CZT detectors	3.17
2×2×2 array with 20mm×20mm×5mm CZT detectors	4.36
2×2×2 array with 20mm×20mm×7.5mm CZT detectors	6.88
2×2×2 array with 25mm×25mm×5mm CZT detectors	7.19

Table 2: Intrinsic photopeak count rates at 662 keV, for each type of detector array, for a 1 mCi ^{137}Cs source located 10 m away from the detector array, on the center axis of the detector array.

5 Detector image resolution

The detector image resolution is defined using the distance of closest approach (DOCA) of an image ring to the true source location. The Compton scattering angle of the first interaction and the positions of the first two interactions of an event define the opening angle and axis direction of a cone. This cone is back-projected onto a sphere which is centered at the detector. The intersection of the cone and the sphere is the Compton image ring, which is a ring-shaped curve that is nearly circular if the radius of the sphere is large compared to the detector length scale. Improving the energy resolution and the position resolution for interactions within the detector crystals improves the image resolution, because reducing the uncertainties in the photon interaction energies and positions reduces the amount by which an image ring is shifted away from the true source location. Figures 6 - 12 show the simulated DOCA distributions for both types of z resolution for each type of detector array. For each simulated DOCA distribution, the source is a 662 keV point source located 10 meters away from the detector array, on the center axis of the detector array.

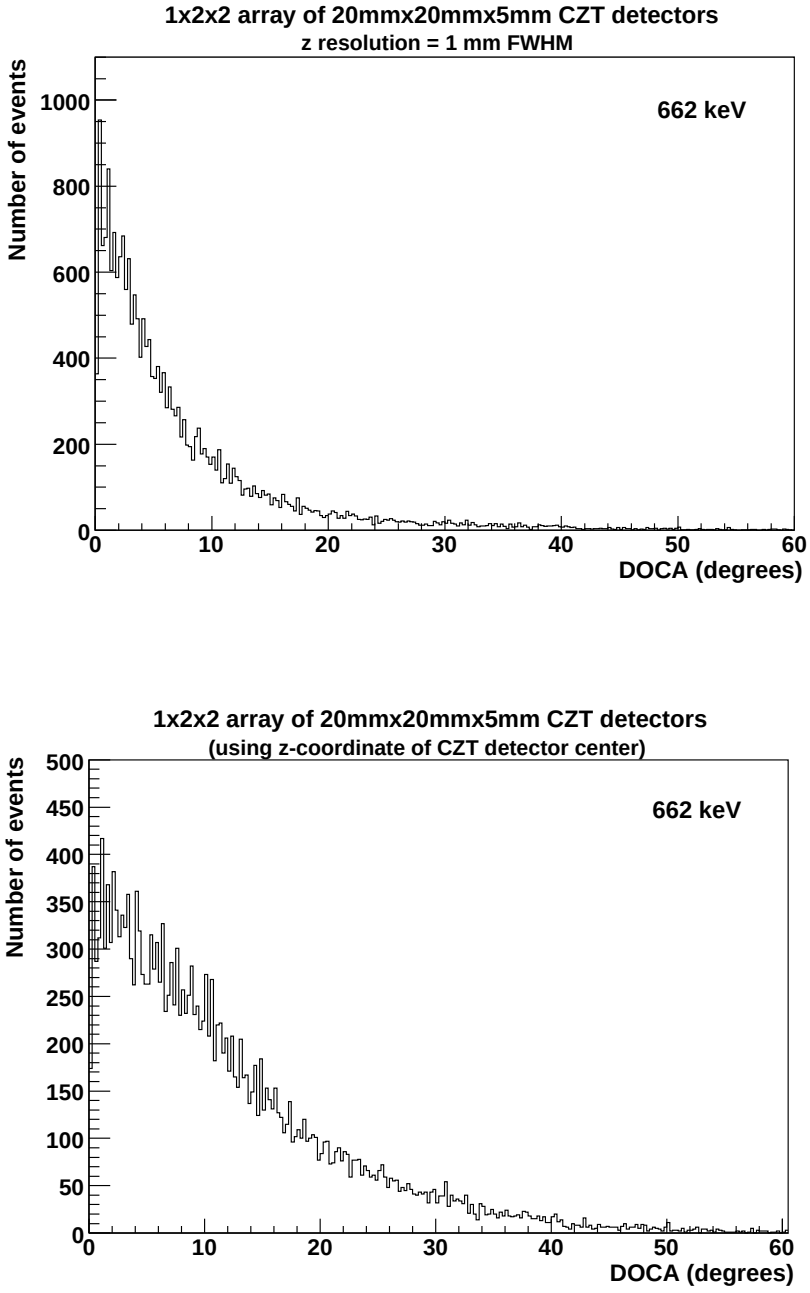

Figure 6: Simulated DOCA distributions for the $1\times2\times2$ array of 20 mm$\times$20 mm$\times$5 mm CZT detectors, for a 662 keV point source located 10 m away from the detector array, on the center axis of the detector array, with the exact z coordinate for each interaction smeared using a Gaussian probability distribution with a FWHM of 1 mm (top), and with the exact z coordinate for each interaction replaced by the z coordinate of the center of the CZT detector containing the interaction (bottom).

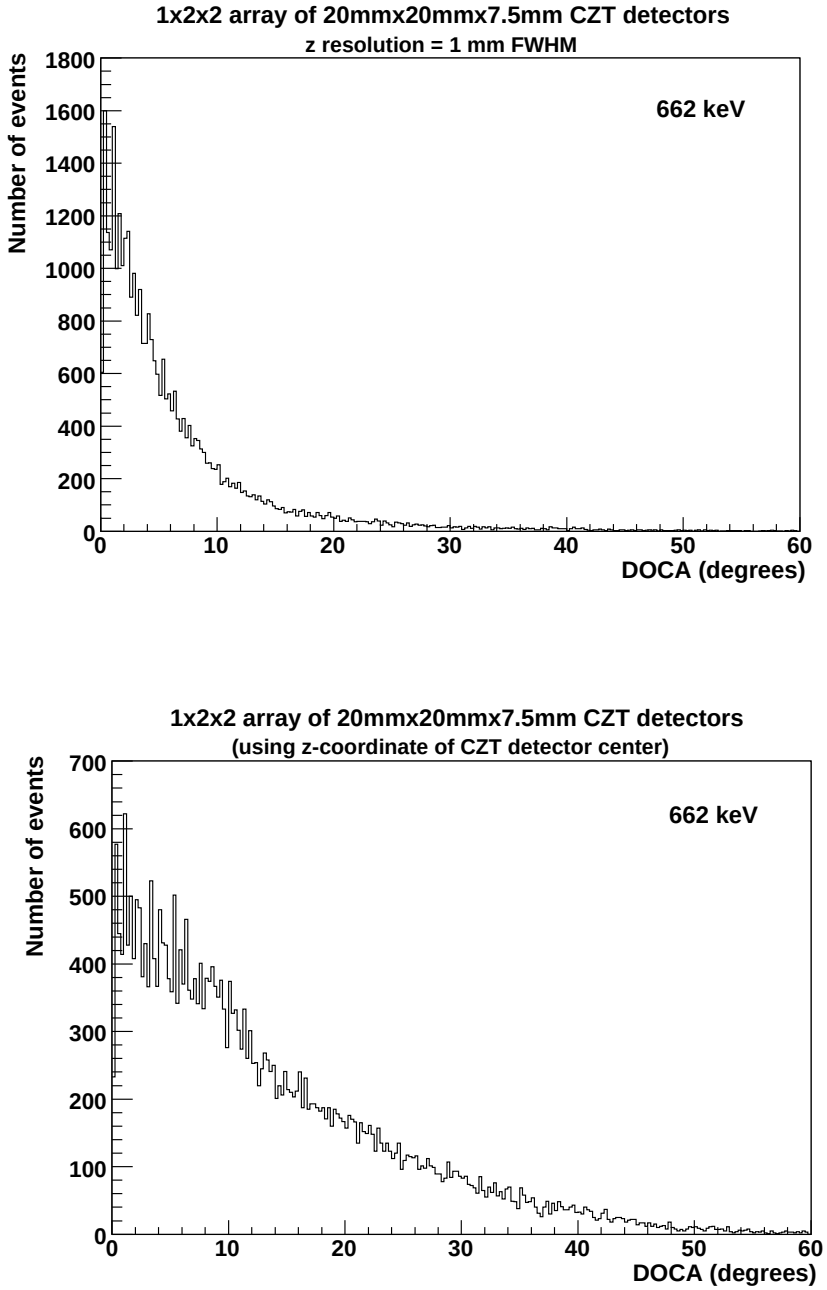

Figure 7: Simulated DOCA distributions for the $1\times2\times2$ array of 20 mm$\times$20 mm$\times$7.5 mm CZT detectors, for a 662 keV point source located 10 m away from the detector array, on the center axis of the detector array, with the exact z coordinate for each interaction smeared using a Gaussian probability distribution with a FWHM of 1 mm (top), and with the exact z coordinate for each interaction replaced by the z coordinate of the center of the CZT detector containing the interaction (bottom).

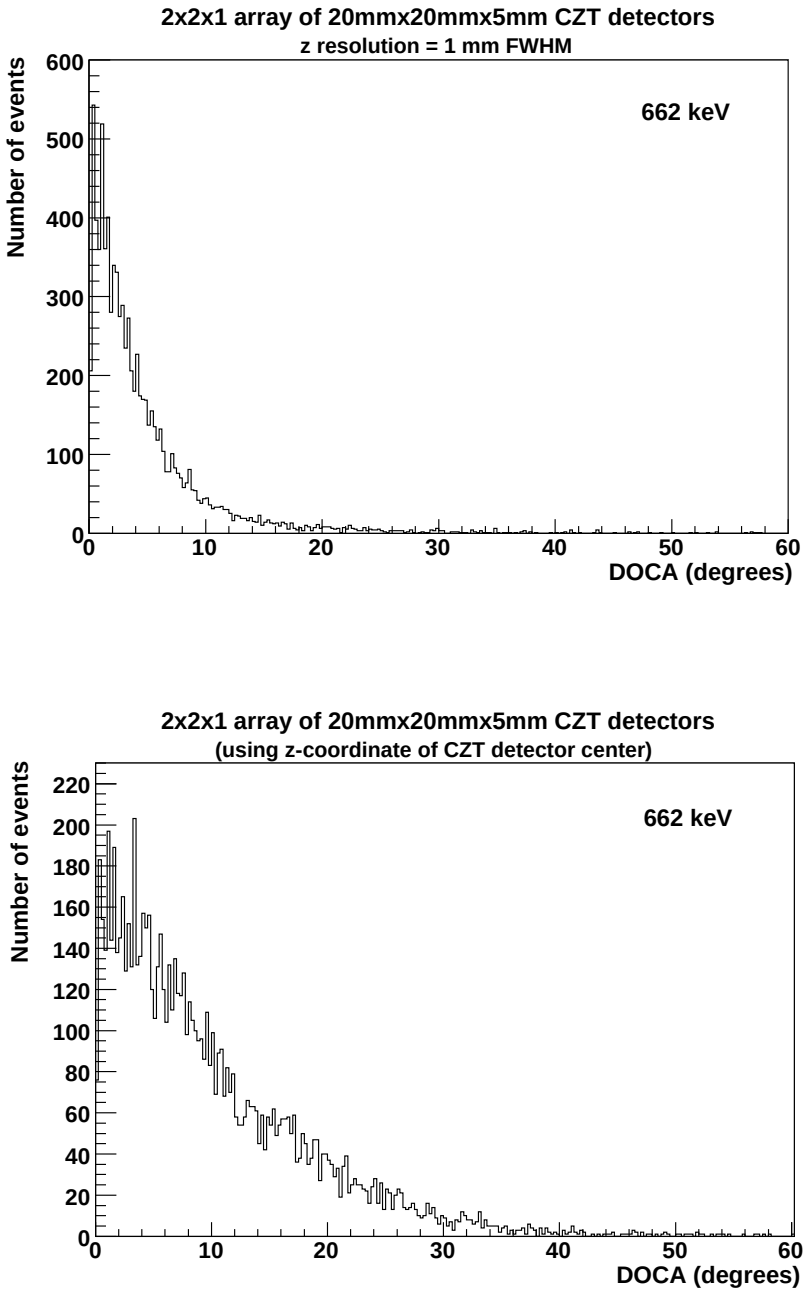

Figure 8: Simulated DOCA distributions for the $2\times2\times1$ array of 20 mm$\times$20 mm$\times$5 mm CZT detectors, for a 662 keV point source located 10 m away from the detector array, on the center axis of the detector array, with the exact z coordinate for each interaction smeared using a Gaussian probability distribution with a FWHM of 1 mm (top), and with the exact z coordinate for each interaction replaced by the z coordinate of the center of the CZT detector containing the interaction (bottom).

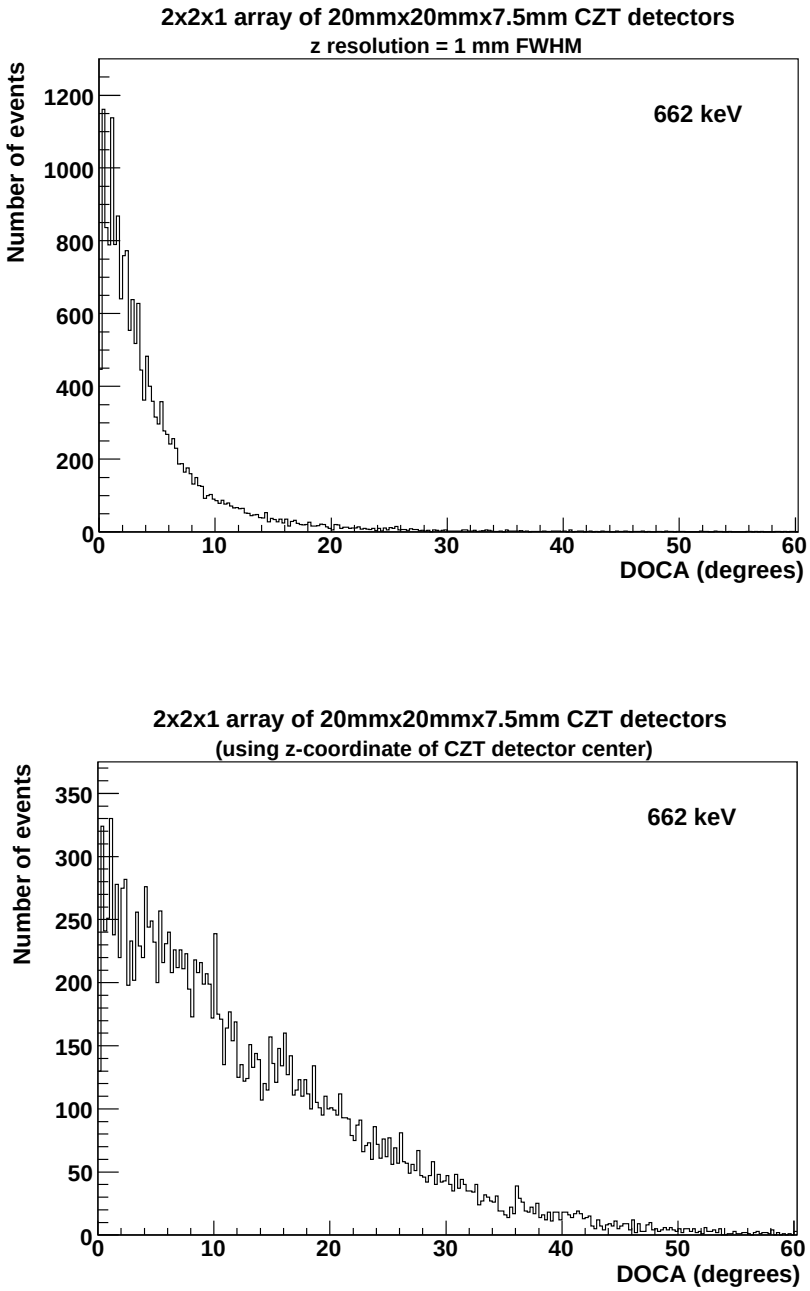

Figure 9: Simulated DOCA distributions for the $2\times2\times1$ array of 20 mm$\times$20 mm$\times$7.5 mm CZT detectors, for a 662 keV point source located 10 m away from the detector array, on the center axis of the detector array, with the exact z coordinate for each interaction smeared using a Gaussian probability distribution with a FWHM of 1 mm (top), and with the exact z coordinate for each interaction replaced by the z coordinate of the center of the CZT detector containing the interaction (bottom).

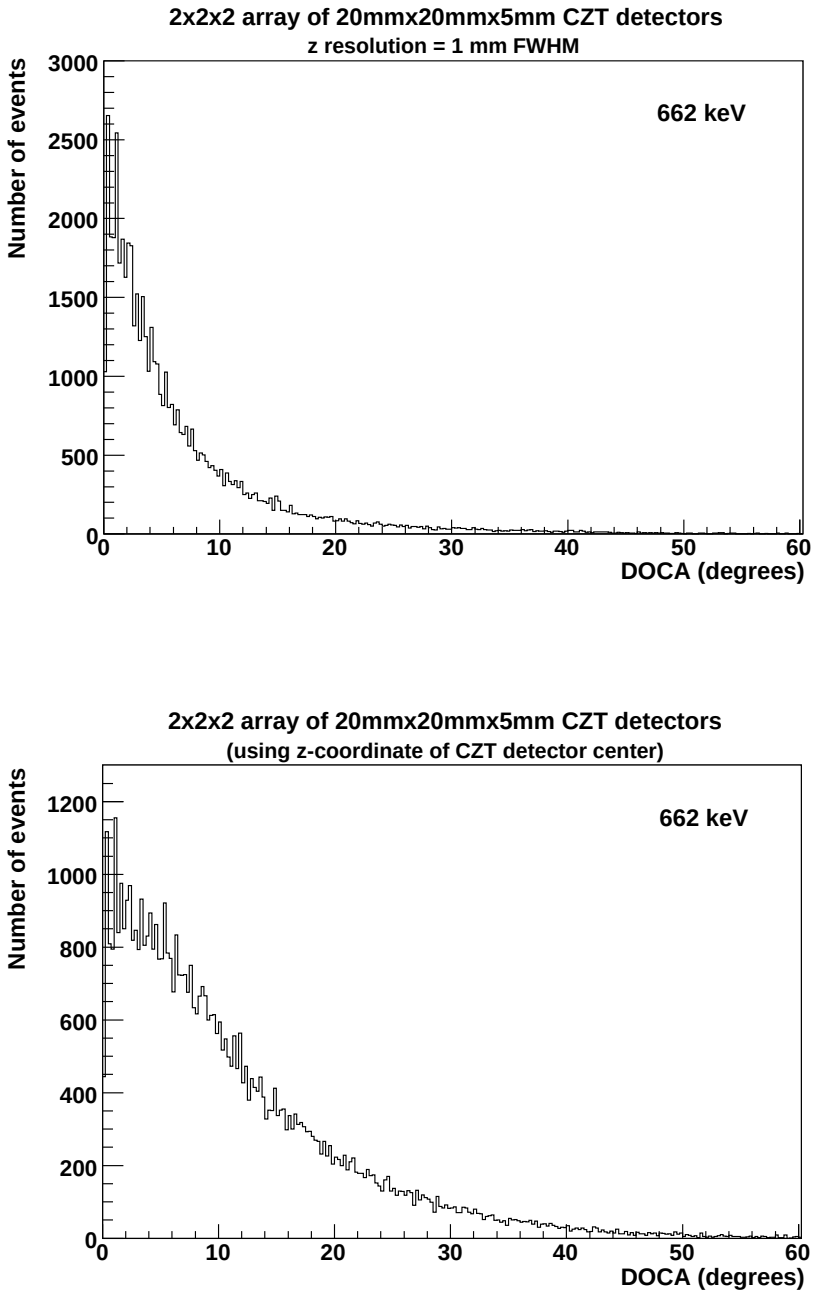

Figure 10: Simulated DOCA distributions for the $2\times2\times2$ array of 20 mm$\times$20 mm$\times$5 mm CZT detectors, for a 662 keV point source located 10 m away from the detector array, on the center axis of the detector array, with the exact z coordinate for each interaction smeared using a Gaussian probability distribution with a FWHM of 1 mm (top), and with the exact z coordinate for each interaction replaced by the z coordinate of the center of the CZT detector containing the interaction (bottom).

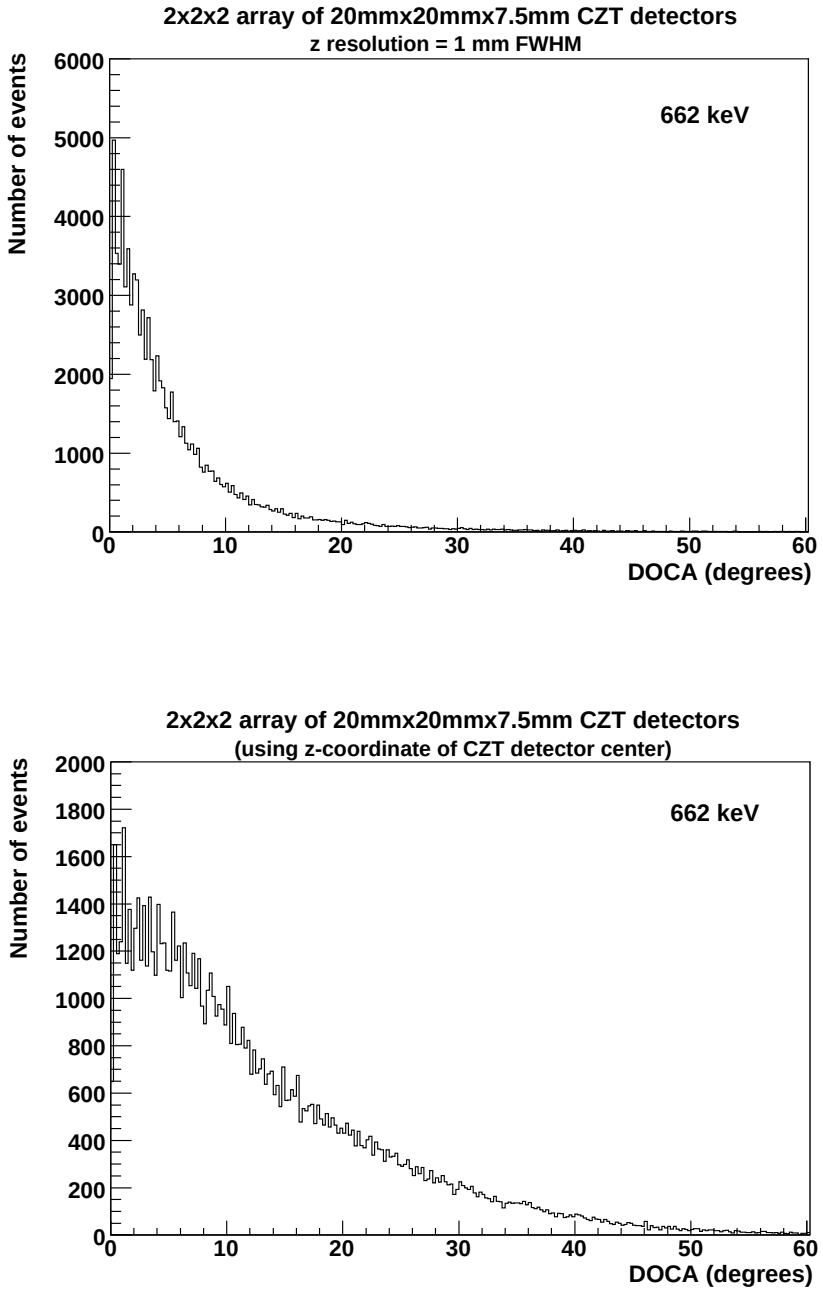

Figure 11: Simulated DOCA distributions for the $2\times2\times2$ array of 20 mm$\times$20 mm$\times$7.5 mm CZT detectors, for a 662 keV point source located 10 m away from the detector array, on the center axis of the detector array, with the exact z coordinate for each interaction smeared using a Gaussian probability distribution with a FWHM of 1 mm (top), and with the exact z coordinate for each interaction replaced by the z coordinate of the center of the CZT detector containing the interaction (bottom).

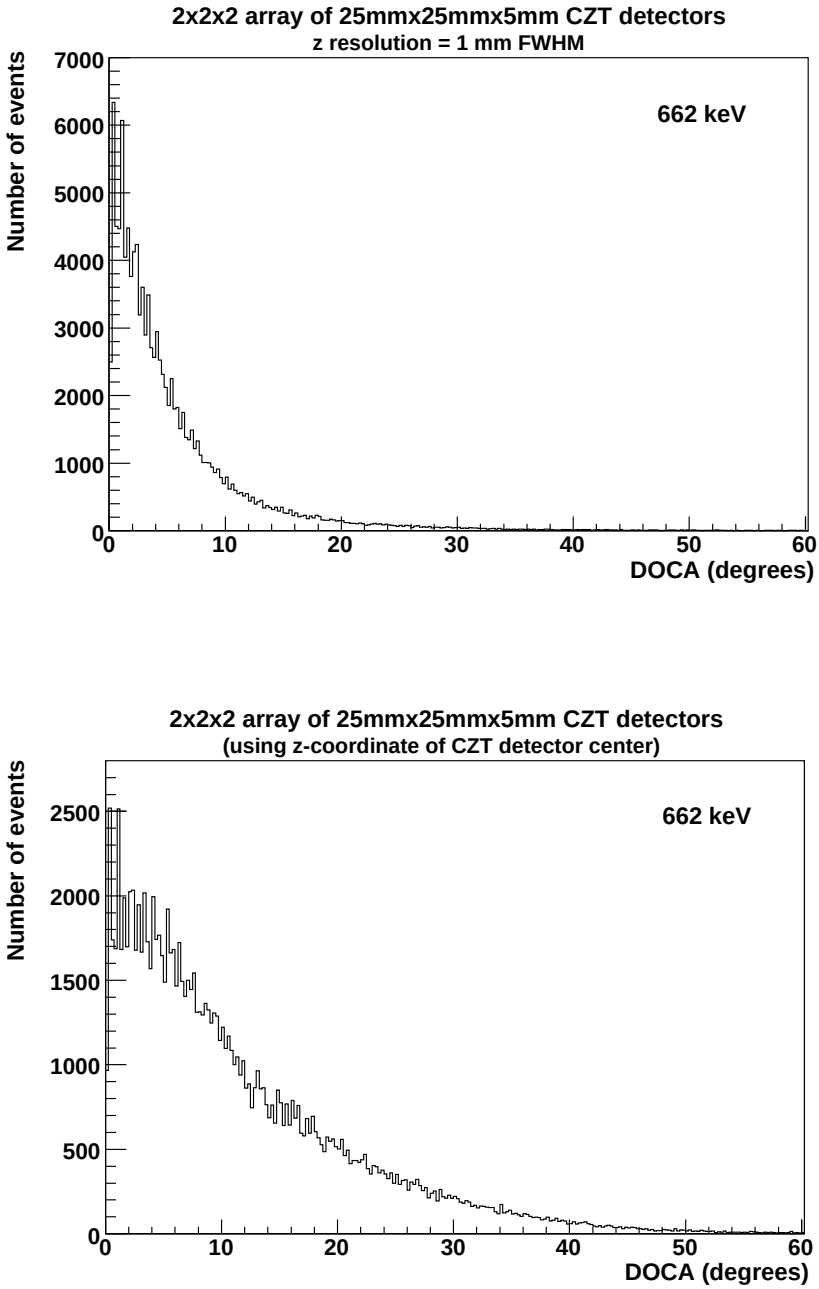

Figure 12: Simulated DOCA distributions for the $2\times2\times2$ array of 25 mm$\times$25 mm$\times$5 mm CZT detectors, for a 662 keV point source located 10 m away from the detector array, on the center axis of the detector array, with the exact z coordinate for each interaction smeared using a Gaussian probability distribution with a FWHM of 1 mm (top), and with the exact z coordinate for each interaction replaced by the z coordinate of the center of the CZT detector containing the interaction (bottom).

6 Imaging efficiency

The imaging efficiency at a particular energy is defined as the number of events in the signal DOCA distribution within the signal region, divided by the total number of signal events incident upon the detector array at the particular energy. The signal region radius is defined by specifying a particular number of degrees along the signal DOCA distribution. Imaged events must pass the following event selection requirements. The event energy deposited in the detector crystals must be within a ± 13 keV energy-cut window centered on the initial generated source photon energy. An event must produce at least two interactions in the detector crystals to be imaged. The first two interactions give the directional information of the incident photon. The total energy deposition for an event is the sum of all energy deposits for all interactions within the detector crystals. If the first two interactions for an event occur within the same pixel, then that event is rejected. If the first two interactions for an event are both within the same detector crystal, then the two interactions must be separated by at least 4 pixel widths.

Table 3 shows the results for the imaging efficiencies at 662 keV for each type of detector array, in which the exact *z* coordinate for each interaction is smeared using a Gaussian distribution with a FWHM of 1 mm. This *z* resolution model produces a sufficiently narrow DOCA distribution such that most of the signal events are contained within a signal region radius of 10 degrees. Thus, increasing the signal region radius from 10 degrees to 30 degrees does not produce a large increase in imaging efficiency.

Table 4 shows the imaging efficiencies at 662 keV for each type of detector array, in which the exact *z* coordinate for each interaction is replaced by the *z* coordinate of the center of the CZT detector containing the interaction. This *z* resolution model produces a sufficiently wide DOCA distribution such that a large fraction of the signal events in the DOCA distribution are between 10 degrees and 30 degrees. This causes a significant increase in imaging efficiency if the signal region radius is increased from 10 degrees to 30 degrees.

Detector array type	Imaging efficiency with signal region radius of 30 degrees	Imaging efficiency with signal region radius of 10 degrees
1×2×2 array with 20mm×20mm×5mm CZT detectors	1.8 %	1.5 %
1×2×2 array with 20mm×20mm×7.5mm CZT detectors	2.9 %	2.4 %
2×2×1 array with 20mm×20mm×5mm CZT detectors	0.4 %	0.3 %
2×2×1 array with 20mm×20mm×7.5mm CZT detectors	0.8 %	0.7 %
2×2×2 array with 20mm×20mm×5mm CZT detectors	2.4 %	1.9 %
2×2×2 array with 20mm×20mm×7.5mm CZT detectors	4.0 %	3.4 %
2×2×2 array with 25mm×25mm×5mm CZT detectors	3.3 %	2.8 %

Table 3: Imaging efficiencies at 662 keV for each type of detector array, in which the exact *z* coordinate for each interaction is smeared using a Gaussian distribution with a FWHM of 1 mm.

Detector array type	Imaging efficiency with signal region radius of 30 degrees	Imaging efficiency with signal region radius of 10 degrees
1×2×2 array with 20mm×20mm×5mm CZT detectors	1.8 %	1.0 %
1×2×2 array with 20mm×20mm×7.5mm CZT detectors	2.7 %	1.5 %
2×2×1 array with 20mm×20mm×5mm CZT detectors	0.4 %	0.2 %
2×2×1 array with 20mm×20mm×7.5mm CZT detectors	0.8 %	0.4 %
2×2×2 array with 20mm×20mm×5mm CZT detectors	2.3 %	1.4 %
2×2×2 array with 20mm×20mm×7.5mm CZT detectors	3.7 %	2.1 %
2×2×2 array with 25mm×25mm×5mm CZT detectors	3.1 %	1.9 %

Table 4: Imaging efficiencies at 662 keV for each type of detector array, in which the exact z coordinate for each interaction is replaced by the z coordinate of the center of the CZT detector containing the interaction.

7 Imaging count rate

The imaging count rates are calculated for each type of detector array, for a 1 mCi ^{137}Cs source located 10 meters away from the detector array, on the center axis of the detector array. These results include the fact that the branching ratio is 85% for a ^{137}Cs decay to emit a 662 keV photon. Note that at a distance of 10 meters, a 1 mCi ^{137}Cs source generates 662 keV photons at a rate of 2.50 photons/second/cm^2.

Table 5 shows the imaging count rates at 662 keV for each type of detector array, in which the exact *z* coordinate for each interaction is smeared using a Gaussian distribution with a FWHM of 1 mm. This *z* resolution model produces a sufficiently narrow DOCA distribution such that most of the signal events are contained within a signal region radius of 10 degrees. Thus, increasing the signal region radius from 10 degrees to 30 degrees does not produce a large increase in imaging count rate.

Table 6 shows the imaging count rates at 662 keV for each type of detector array, in which the exact *z* coordinate for each interaction is replaced by the *z* coordinate of the center of the CZT detector containing the interaction. This *z* resolution model produces a sufficiently wide DOCA distribution such that a large fraction of the signal events in the DOCA distribution are between 10 degrees and 30 degrees. This causes a significant increase in imaging count rate if the signal region radius is increased from 10 degrees to 30 degrees.

Detector array type	Imaging count rate with signal region radius of 30 degrees (counts/second)	Imaging count rate with signal region radius of 10 degrees (counts/second)
1×2×2 array with 20mm×20mm×5mm CZT detectors	0.36	0.30
1×2×2 array with 20mm×20mm×7.5mm CZT detectors	0.58	0.48
2×2×1 array with 20mm×20mm×5mm CZT detectors	0.16	0.12
2×2×1 array with 20mm×20mm×7.5mm CZT detectors	0.32	0.28
2×2×2 array with 20mm×20mm×5mm CZT detectors	0.96	0.76
2×2×2 array with 20mm×20mm×7.5mm CZT detectors	1.60	1.36
2×2×2 array with 25mm×25mm×5mm CZT detectors	2.06	1.75

Table 5: Imaging count rates at 662 keV for each type of detector array, for a 1 mCi ^{137}Cs source located 10 m away from the detector array, on the center axis of the detector array, in which the exact *z* coordinate for each interaction is smeared using a Gaussian distribution with a FWHM of 1 mm.

Detector array type	Imaging count rate with signal region radius of 30 degrees (counts/second)	Imaging count rate with signal region radius of 10 degrees (counts/second)
1×2×2 array with 20mm×20mm×5mm CZT detectors	0.36	0.20
1×2×2 array with 20mm×20mm×7.5mm CZT detectors	0.54	0.28
2×2×1 array with 20mm×20mm×5mm CZT detectors	0.16	0.08
2×2×1 array with 20mm×20mm×7.5mm CZT detectors	0.32	0.16
2×2×2 array with 20mm×20mm×5mm CZT detectors	0.92	0.56
2×2×2 array with 20mm×20mm×7.5mm CZT detectors	1.48	0.84
2×2×2 array with 25mm×25mm×5mm CZT detectors	1.94	1.19

Table 6: Imaging count rates at 662 keV for each type of detector array, for a 1 mCi ^{137}Cs source located 10 m away from the detector array, on the center axis of the detector array, in which the exact z coordinate for each interaction is replaced by the z coordinate of the center of the CZT detector containing the interaction.